THE JOURNAL OF BIOLOGICAL CHEMISTRY VOL. 287, NO. 10, pp. 7661–7674, March 2, 2012
© 2012 by The American Society for Biochemistry and Molecular Biology, Inc. Published in the U.S.A.

Structural Dynamics of C-domain of Cardiac Troponin I Protein in Reconstituted Thin Filament*

Received for publication, July 17, 2011, and in revised form, December 6, 2011 Published, JBC Papers in Press, December 28, 2011, DOI 10.1074/jbc.M111.281600

Zhiqun Zhou[‡1], King-Lun Li[§1], Daniel Rieck[§1], Yexin Ouyang[‡§], Murali Chandra[§], and Wen-Ji Dong[‡§2]

From the [‡]Department of Veterinary and Comparative Anatomy Pharmacology and Physiology and [§]Voiland School of Chemical Engineering and Bioengineering, Washington State University, Pullman, Washington 99164

Background: The kinetics and dynamics of the C-domain of cTnI were studied.
Results: Fluorescence anisotropy data show support for the fly casting model and a fourth state of thin filament activation.
Conclusion: The fly casting model holds true in the thin filament, but the presence of S1 modulates the process.
Significance: Our study provides information on the role of the cTnI C-domain in thin filament regulation.

The regulatory function of cardiac troponin I (cTnI) involves three important contiguous regions within its C-domain: the inhibitory region (IR), the regulatory region (RR), and the mobile domain (MD). Within these regions, the dynamics of regional structure and kinetics of transitions in dynamic state are believed to facilitate regulatory signaling. This study was designed to use fluorescence anisotropy techniques to acquire steady-state and kinetic information on the dynamic state of the C-domain of cTnI in the reconstituted thin filament. A series of single cysteine cTnI mutants was generated, labeled with the fluorophore tetramethylrhodamine, and subjected to various anisotropy experiments at the thin filament level. The structure of the IR was found to be less dynamic than that of the RR and the MD, and Ca^{2+} binding induced minimal changes in IR dynamics: the flexibility of the RR decreased, whereas the MD became more flexible. Anisotropy stopped-flow experiments showed that the kinetics describing the transition of the MD and RR from the Ca^{2+}-bound to the Ca^{2+}-free dynamic states were significantly faster (53.2–116.8 s^{-1}) than that of the IR (14.1 s^{-1}). Our results support the fly casting mechanism, implying that an unstructured MD with rapid dynamics and kinetics plays a critical role to initiate relaxation upon Ca^{2+} dissociation by rapidly interacting with actin to promote the dissociation of the RR from the N-domain of cTnC. In contrast, the IR responds to Ca^{2+} signals with slow structural dynamics and transition kinetics. The collective findings suggested a fourth state of activation.

In striated muscle, Ca^{2+}-dependent activation is traced to the thin filament, a double helical, filamentous protein supercomplex built from repeats of the heterotrimeric troponin complex, tropomyosin (Tm),[3] and actin bound together in a ratio of 1:1:7, respectively (1, 2). Cardiac troponin (cTn) is formed from subunits troponin C (cTnC), troponin I (cTnI), and troponin T (cTnT). cTnC binds Ca^{2+}, cTnI binds actin and inhibits actomyosin ATPase in relaxed muscle, and cTnT anchors the cTn complex on the actin filament. In relaxed myocardium under a $\sim 10^{-6}$ M resting concentration of Ca^{2+}, cTnI-Tm acts as a regulatory switch to prevent cross-bridge formation between actin and myosin heads (myosin subfragment-1 (S1)) through steric blocking of myosin-binding sites on actin (3–5). To activate actomyosin ATPase and force generation, intracellular [Ca^{2+}] rises to saturate the regulatory sites in cTn, inducing a series of critical intramolecular and intermolecular structural changes in the thin filament. These structural changes include the opening/closing of the N-domain of cTnC (6, 7), changes in the conformation of the C-domain of cTnI (C-cTnI) (8–10), switching of the inhibitory and regulatory regions of cTnI from interacting with actin to interacting with cTnC (11), and movement of Tm on the actin surface (12), which permits strong cross-bridge cycling between actin and myosin. These Ca^{2+}-dependent transitions in dynamic state are the molecular basis for cardiac thin filament regulation.

Naturally, dynamic interactions among the thin filament proteins form a main feature of the Ca^{2+}-dependent activation of cardiac muscle with multiple transitions in dynamic state occurring at the thin filament protein interfaces (13, 14). Some interactions have been shown to be notably rigid and invariant in terms of conformational dynamics, whereas others involve structural regions marked by flexibility and prone to facilitating conformational changes (15, 16). Among the thin filament proteins, cTnI is unique in that it exhibits a remarkable diversity in the conformational dynamics of its subdomains (13), enabling it to take part in both rigid interactions that enforce protein localization and more transient interactions associated with functional conformational changes. For example, although the cTn complex is directly anchored to the actin filament through an interaction between the N-domain (TnT1) of cTnT and Tm occurring on the actin surface, cTnI is in turn anchored to cTnT (14); the crystal structure of the core domain of cTn

* This work was supported, in whole or in part, by National Institutes of Health Grants HL80186 (to W.-J. D.), HL80186-5S1 (to W.-J. D.), and HL075643 (to M. C.). This work was also supported by the M. J. Murdock Charitable Trust (to W.-J. D.).

[1] These authors made equal contributions to this work.

[2] To whom correspondence should be addressed: Dept. of Veterinary and Comparative Anatomy Pharmacology and Physiology, 205 Wegner Hall, Washington State University, Pullman, WA 99164. Fax: 509-335-4650; E-mail: wdong@vetmed.wsu.edu.

[3] The abbreviations used are: Tm, tropomyosin; cTn, cardiac troponin; C-cTnI, C-domain of cTnI; N-cTnC, N-domain of cTnC; IR, inhibitory region; RR, regulatory region; MD, mobile domain; S1, myosin subfragment-1; TAMRA, tetramethylrhodamine; IAANS, 2-(4′(iodoacetamide)anilino)naphthalene-6-sulfonic acid sodium salt; mA, units of millianisotropy, equal to the fractional and unitless measured anisotropy value multiplied by 1000.

under Ca^{2+}-saturated conditions showed that two helices in the N-domain of cTnI (residues 40–80 and 90–130, respectively) strongly interact with the C-domain of cTnC and the cTnT helix domain of cTnT (residues 226–276), respectively, to form two extended helices (17). Similarly, cTnI occupies a central role in the Ca^{2+}-dependent transitions in the dynamic state of thin filament proteins that are associated with regulatory function through its alternating interactions with cTnC (6, 7) and actin (15, 18) under various biochemical conditions, and expectedly, this functional behavior is traced to the C-domain of cTnI (15, 16).

Three contiguous regions making essential contributions to regulatory function have been identified within C-cTnI: the inhibitory region (IR), the regulatory region (RR), and the mobile domain (MD). The IR (residues 130–150) is mainly responsible for inhibiting muscular contraction through its binding to actin in the absence of Ca^{2+}. The RR (residues 151–167) plays a triggering role in the thin filament activation process by binding to the N-domain of cTnC once Ca^{2+} has bound to the regulatory site of cTnC (6, 7). The MD (residues 167–210) stabilizes the interaction between cTnI and actin occurring in the absence of Ca^{2+} (15, 18). Because of these different mechanistic roles, it is expected that each region may be marked by unique structural dynamics and kinetics when participating in thin filament regulation. Affirming this notion, it has been shown that structural dynamics of these regions and particularly the MD significantly change in response to Ca^{2+}-induced thin filament activation (15, 16). It has recently been proposed that the highly dynamic nature of the MD may play a critical role in regulating thin filament relaxation by promoting the binding of the IR to actin through "fly casting" activity (13). However, detailed information on the structural dynamics of each functional region under different biochemical states and how their dynamics change during the course of structural transitions has remained elusive especially in the context of the thin filament.

Anisotropy is a technique with the potential to provide this missing information. When a fluorophore is attached to a protein, the motion of the fluorophore can be correlated to global protein motion or the structural flexibility of the region to which the probe has been attached. Briefly, fluorescence anisotropy measurements are based on the principle of the photoselective excitation of fluorophores by polarized light. Upon exposure to a polarized light source, fluorophores with dipole transition moments oriented parallel to the electric vector of incoming light will be selectively excited, resulting in a partially oriented population of fluorophore as well as a partially polarized fluorescence emission. Fluorescence anisotropy is then defined by the relative fluorescence intensity of the vertically polarized emission with respect to the intensity of the total emission (19). In principle, the steady-state fluorescence anisotropy (r) of the fluorophore-labeled protein can be approximated using Perrin's equation (20, 21),

$$r = r_0 \cdot (1 + \tau \cdot \phi^{-1})^{-1} \quad \text{(Eq. 1)}$$

where r_0 is the fundamental anisotropy, τ is the fluorescence lifetime, and Φ is the rotational correlation time of the fluorophore that can be determined by time-resolved fluorescence anisotropy measurements. The anisotropy for a chosen fluorophore will be primarily determined by the correlation time, which strongly depends on the motion of the fluorophore. Because fluorophore tumbling is very fast compared with global or regional protein motion, the overall correlation time can be unambiguously resolved to obtain the contribution from protein dynamics to total anisotropy. Therefore steady-state and time-resolved fluorescence anisotropy can provide not only a qualitative assessment of the dynamics of C-cTnI but also a quantitative measure of the conformational flexibility and structural transition kinetics of each functional region of C-cTnI during regulation.

In this study, we hypothesized accordingly that anisotropy probes placed at different locations along the C-domain of cTnI would report regional dynamic behavior. If this hypothesis were validated, new insights into the mechanistic role of each C-cTnI functional region when incorporated into the thin filament could then be gained. To test our hypothesis, we used fluorescence anisotropy measurements to acquire detailed information on probe motion within each functional region under different activation states of the thin filament. Upon finding that probe motion did indeed reflect regional conformational dynamics, fluorescence quenching and stopped-flow kinetic measurements were used to further examine regional structural flexibility, solvent accessibility, and dynamic state transition kinetics in terms of Ca^{2+} dependence with or without S1 present. Our combined results provide strong support for the fly casting model, suggesting that an unstructured MD rapidly reacts to Ca^{2+} dissociation to initiate the relaxation process followed by slower structural transitions involving the RR and then the IR. Interestingly, a fourth state of activation (22) is also suggested by our results involving S1-dependent effects on C-cTnI regional flexibility and on its dynamic state transitions induced by Ca^{2+} dissociation.

EXPERIMENTAL PROCEDURES

Protein Preparation—Wild-type recombinant cTnC and cTnT were overexpressed in *Escherichia coli* strain BL21(DE3) cells and purified as described previously (6, 8, 11). Using the GeneTailor™ Site-Directed Mutagenesis System (Invitrogen), a rat cDNA clone of wild-type cTnI subcloned into the plasmid pSBETa was used as a template DNA to convert the two endogenous cysteines at positions 81 and 98 into Ser and Ile, respectively, thus generating a cysteine-less cTnI(C81S/C98I) mutant. The cysteine-less mutant was then used as a template to create the following single cysteine cTnI mutants: T130C, L145C, S151C, L160C, S167C, V177C, I182C, V189C, S200C, and E210C. The mutant clone construction, protein expression, purification, and characterization have been described in detail previously (23). Cardiac Tm was purified from bovine heart (24). Actin (25) and S1 from the chymotryptic digestion of myosin (26) were obtained from rabbit skeletal muscle.

The cysteine residue of each single cysteine cTnI mutant was modified with either the fluorophore TAMRA or IAANS based on slight modifications of procedures described previously (6, 8). Briefly, single cysteine cTnI was incubated with a 5-fold molar excess of fluorophore in the presence of 6 M urea at 4 °C

overnight. The reaction was terminated by adding 1 mM DTT to the reaction solution. Unreacted fluorophore was removed by passing the solution through a CM-Sepharose column and subsequently washing the column with a buffer containing 6 M urea, 30 mM citric acid, pH 6.0, 1 mM EDTA, and 1 mM DTT. Labeled cTnI was eluted with the same buffer plus 0.3 M KCl. The labeled cTnI protein was further dialyzed against a buffer containing 3 M urea, 50 mM Tris-HCl, pH 7.4, 1 mM DTT, 1 mM EDTA, and 0.4 mM NaCl. The ratio of labeled to total cTnI was determined using $\epsilon_{580\ nm} = 95{,}000\ cm^{-1}{\cdot}M^{-1}$ for TAMRA and $\epsilon_{325\ nm} = 24{,}900\ cm^{-1}{\cdot}M^{-1}$ for IAANS. Labeling ratios for all of the protein modifications involved in this study were >95%.

Reconstitution of cTn complexes from wild-type cTnC, TAMRA- or IAANS-labeled cTnI, and wild-type cTnT was carried out in 6 M urea at a molar ratio of 1.2:1.0:1.2 cTnC:cTnI:cTnT following a procedure reported previously (27). Reconstituted cTn containing one of the modified cTnI mutants was then used together with Tm and actin to form the reconstituted thin filament for use in anisotropy experiments (27). cTnI mutants were also incorporated into detergent-skinned muscle fibers (28), and the following experiments were performed to test for any effects on protein stability and functional integrity caused by cTnI mutations and probe modifications: 1) SDS-PAGE and native gel analysis, 2) ATPase activity measurements, and 3) measurement of the force-Ca^{2+} relationship under steady-state conditions. The gel analysis of reconstituted troponin complexes (data not shown) and skinned muscle fiber measurements (Table 1) showed no evidence of protein degradation or functional loss, suggesting that the effects of our mutations and modifications of cTnI on Ca^{2+}-dependent regulatory activity were negligible.

Fluorescence Measurements—Steady-state fluorescence anisotropy measurements were taken at 20 °C on an ISS, Inc. PC1 photon-counting spectrofluorometer using a band pass of 3 nm on both the excitation and emission monochromators. Samples containing 1 μM protein in the working buffer (composed of 30 mM MOPS, pH 7.0, 5 mM $MgCl_2$, 0.15 M KCl, 1 mM DTT, and 1 mM EGTA) were tested in the presence and absence of 3 mM $CaCl_2$ both with and without ADP-Mg^{2+}-S1 present. Samples were excited with vertically polarized 495 nm light, and using L-format detection, the fluorescence intensities of the vertically ($I_{\parallel}$) and horizontally ($I_{\perp}$) polarized emissions from TAMRA-labeled samples were simultaneously recorded at a wavelength of 545 nm. The steady-state anisotropy r was then calculated using Equation 2,

$$< r > = (I_{\parallel} - GI_{\perp}) \cdot (I_{\parallel} + 2GI_{\perp})^{-1} \qquad \text{(Eq. 2)}$$

where G is a scale factor used to correct for the polarization bias in the detection system. G can be experimentally determined from

$$G = I_{HV} \cdot I_{HH}^{-1} \qquad \text{(Eq. 3)}$$

where I_{HV} is the fluorescence intensity when the excitation polarizer is kept horizontal and the emission polarizer is vertical, and I_{HH} is the fluorescence intensity when both of the polarizers are kept horizontal. Each anisotropy measurement was repeated 10–15 times, and for every trial, the G-factor was determined. Typically, the G-factors obtained for steady-state measurements were in the range of 0.82–0.88.

Time-resolved anisotropy decays were obtained using a FluoroCube (Horiba Jobin Yvon) lifetime system with an L-format detection arrangement. Vertically and horizontally polarized emissions were monitored at a wavelength of 545 nm from the left channel with vertically polarized 495 nm excitation light supplied from a light-emitting diode with a 1.4-ns pulse width. The anisotropy decays obtained were recorded with TBX picosecond photon detection modules and fitted with a multiexponential function (29),

$$r(t) = r_0 \sum \alpha_i \cdot \exp(-t \cdot \Phi_i^{-1}) \qquad \text{(Eq. 4)}$$

where r_0 is the limiting anisotropy, and the α_i values are the fractional amplitudes of each correlation time (Φ_i) in the anisotropy decay. Data analysis was performed using anisotropy analysis software provide by Horiba Jobin Yvon.

Fluorescence Quenching—Because TAMRA fluorescence was insensitive to the neutrally charged quencher acrylamide, fluorescence quenching experiments relied instead on single cysteine cTnI mutants labeled with the spectrally inferior but quenching-susceptible fluorophore IAANS. Acrylamide-dependent fluorescence quenching was determined from IAANS fluorescence recorded using an ISS, Inc. PC1 photon-counting spectrofluorometer equipped with a microtitrator held at 20 ± 0.1 °C (6, 30). For the quenching titration, 1.2 ml of sample was excited with 325 nm light, and the emission was monitored at 480 nm. A total of 44 data points were acquired after successively injecting aliquots of 10 μl each of 6 M acrylamide prepared in sample buffer with 10 s of holding time for each injection made. Samples contained 1 μM thin filaments reconstituted with labeled cTnI and were prepared in a buffer containing 30 mM MOPS, pH 7, 5 mM $MgCl_2$, 1 mM EGTA, 1 mM DTT, and 0.2 M KCl. Because of nonlinearity especially at high concentrations of acrylamide, suggesting the presence of apparent static quenching, quenching data were analyzed by the modified Stern-Volmer equation (19),

$$F_0 \cdot F^{-1} = (1 + K_{SV} \cdot [Q]) e^{V[Q]} \qquad \text{(Eq. 5)}$$

where F_0 and F are the fluorescence intensities in the absence and presence of quencher, respectively; $[Q]$ is the molar concentration of quencher; K_{SV} is the Stern-Volmer dynamic quenching constant; and V represents a volume immediately surrounding excited IAANS within which static quenching occurs.

Stopped-flow Kinetic Measurements—Stopped flow was used to examine the kinetics associated with changes in the structural dynamics induced by Ca^{2+} dissociation for each functional region within C-cTnI (31). Experiments were performed with a T format KinTek stopped-flow spectrometer with a 1.8-ms dead time. Ca^{2+}-saturated thin filament samples reconstituted from a TAMRA-labeled cTnI mutant were rapidly mixed with an equal volume of a buffer containing an excess amount of 1,2-bis(2-aminophenoxy)ethane-*N*,*N*,*N*′,*N*′-tetraacetic acid (a Ca^{2+} chelator) (32). The mixed sample was then excited by vertically polarized light (490 nm), and kinetic traces of the vertically and horizontally polarized emissions from the

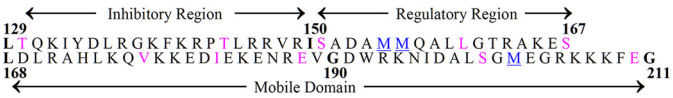

SCHEME 1. **Amino acid sequence of C-domain of rat cTnI.** *Pink* residues are the amino acids that were replaced by cysteine for subsequent TAMRA/IAANS labeling.

sample were simultaneously collected with a T format detection system equipped with 500-nm cutoff filters to block excitation light. The two polarized intensity traces were converted into anisotropy traces using Equation 2 and fitted with a sum of exponential functions to determine the rate constants associated with fluorophore tumbling and changes in regional dynamic state. Generally, 8–12 polarized fluorescence traces were collected for each fluorescently labeled single cysteine cTnI mutant. A *G*-factor for each sample was also determined using Equation 3 by exciting it with horizontally polarized excitation light and collecting the kinetic traces of the vertically and horizontally polarized emissions. Typically, *G*-factors for the stopped-flow system were in the range of 0.80–0.85.

RESULTS

In this study we generated 10 cTnI mutants that can be labeled with thiol-reactive anisotropy probes; each mutant contains a single cysteine residue that has been positioned along C-cTnI at either Cys-130 or Cys-145 in the IR; Cys-151, Cys-160, Cys-167, or Cys-177 in the RR; or Cys-182, Cys-189, Cys-200, or Cys-210 in the MD (Scheme 1, *pink* residues). Residue Cys-145 is located in the middle of the IR, whereas residue Cys-160 is located in the middle of the RR of cTnI. Residues Cys-130 and Cys-151 are located at the N-terminal end and C-terminal end of the IR, respectively, whereas residue Cys-167 is located at the C terminus of the RR. Accordingly, we hypothesized that each of the single cysteine cTnI mutants when modified with TAMRA as a fluorescence anisotropy probe would enable us to collect information on the regional structural dynamics and kinetics that would help distinguish the role of each functional region of C-cTnI in thin filament regulation. To test this hypothesis, reliable comparisons of the structural dynamics of different regions in C-cTnI were essential; thus, the endogenous residue Cys-98 was chosen as a reference to be used in control experiments. The residue Cys-98 is part of a helix in the N-domain of cTnI that strongly interacts with the helix domain of cTnT (residues 226–276) to form an extended helix (17). Therefore, it was expected that Ca^{2+}-dependent changes in the regional structural dynamics of the helical domain of cTnI containing residue 98 would be minimal.

It was also imperative to examine the potential for detrimental effects from these mutations and their associated fluorophore modifications on the structure and function of cTnI. Hence, each mutant was exchanged via equilibrium into detergent-skinned muscle fibers wherein it was extensively evaluated for its effect on the regulation of ATPase activity and force development. For each of the cTnI mutants incorporated into detergent-skinned myocardial fibers, we observed a passive tension, maximal tension, ATPase activity level, and Ca^{2+} sensitivity of steady-state force development statistically similar to that of the control (Table 1). In all cases, force levels following

TABLE 1
Properties of myocardial fibers reconstituted with TAMRA-modified cTnI mutants
Sarcomere length = 2.2 μm; T = 22 °C. mN, millinewtons.

cTnI mutants	Tension		ATPase	pCa_{50}
	Maximum	Minimum		
	mN/mm²		*pmol/mm³/s*	
cTnI(WT), control	51.92 ± 1.98	3.23 ± 0.35	236.68 ± 6.73	6.22
$cTnI(Cys\text{-}98)_{TAMRA}$	48.42 ± 1.28	2.94 ± 0.29	236.68 ± 5.91	6.22
$cTnI(T130C)_{TAMRA}$	52.12 ± 1.78	3.66 ± 0.36	214.36 ± 6.61	6.29
$cTnI(L145C)_{TAMRA}$	48.02 ± 1.50	2.75 ± 0.30	219.82 ± 6.73	6.29
$cTnI(S151C)_{TAMRA}$	49.91 ± 1.56	3.84 ± 0.43	217.23 ± 7.73	6.19
$cTnI(L160C)_{TAMRA}$	51.92 ± 1.98	2.97 ± 0.27	236.68 ± 6.73	6.22
$cTnI(S167C)_{TAMRA}$	48.42 ± 1.28	2.77 ± 0.32	236.68 ± 5.91	6.22
$cTnI(V177C)_{TAMRA}$	52.12 ± 1.78	3.16 ± 0.28	214.36 ± 6.61	6.29
$cTnI(V189C)_{TAMRA}$	48.02 ± 1.50	2.94 ± 0.31	219.82 ± 6.73	6.29
$cTnI(S200C)_{TAMRA}$	49.91 ± 1.56	2.81 ± 0.26	217.23 ± 7.73	6.19
$cTnI(E210C)_{TAMRA}$	49.91 ± 1.56	3.39 ± 0.34	217.23 ± 7.73	6.19

exchange with cTnI-cTnT and subsequently reconstitution with cTnC suggested that the extent of mutant cTnI incorporation was >90% (data not shown). This suggested that the point mutations and fluorophore modifications associated with the single cysteine cTnI mutants used in this study exerted negligible effects on the Ca^{2+}-dependent regulatory activity of mutated proteins relative to wild-type cTnI.

Steady-state Anisotropy Measurements—Each TAMRA-labeled cTnI mutant was reconstituted with wild-type cTnC, cTnT, Tm, and actin into a thin filament sample and subjected to steady-state anisotropy experiments to determine the total anisotropy calculated from Equation 2; the results are summarized in Table 2. In addition, fluorescence measurements taken at steady state showed that all samples exhibited a maximal emission at ~545 nm when they were excited with 495 nm light (data not shown). A less than 7% change in the unpolarized total fluorescence intensity was observed for each sample when Ca^{2+} was added to the sample in the absence or presence of strongly bound S1; these changes were considered as not significant.

It is expected that the observed fluorescence anisotropies should be correlated with the structural flexibility of each region to which TAMRA was attached, which should enable us to distinguish functional regions based on their expected flexibilities under different conditions (see "Time-resolved Anisotropy Measurements" for a discussion of the limitations involved). Indeed, probe motion was found to depend upon probe location within the C-domain of cTnI when incorporated into the thin filament, and it responded differently to Ca^{2+} binding based on the region labeled in a manner consistent with the dynamics known for each functional region. For example, in the absence of Ca^{2+}, TAMRA attached to the IR of cTnI showed higher fluorescence anisotropy (360 mA (units of millianisotropy, equal to the fractional and unitless measured anisotropy value multiplied by 1000) for residue 130 and 352 mA for residue 145) than the RR (307–332 mA) and the MD (302–320 mA). Generally speaking, the higher the fluorescence anisotropy for a fluorophore, the less flexible is the region to which it is attached (based on Equations 1 and 2). In the deactivated state, the structure of the IR of cTnI within the thin filament is known to be less dynamic due to its strong binding to the actin filament. In the activated state occurring upon Ca^{2+} binding to

TABLE 2
Total fluorescence anisotropy (FA) of TAMRA-labeled cTnI within reconstituted thin filament in presence/absence of strongly bound S1

Samples	Fluorescence anisotropy							
	Thin filament				Thin filament + S1-ADP			
	Mg^{2+}	Ca^{2+}	ΔFA^a	*p* value[b]	Mg^{2+}	Ca^{2+}	ΔFA^a	*p* value[b]
	mA	*mA*	*mA*		*mA*	*mA*	*mA*	
$cTnI(Cys\text{-}98)_{TAMRA}$	331	329	−2	0.202	328	327	−1	0.254
$cTnI(T130C)_{TAMRA}$	360	360	0	0.396	354	351	−3	0.143
$cTnI(L145C)_{TAMRA}$	352	350	−2	0.132	336	342	6	0.034
$cTnI(S151C)_{TAMRA}$	315	326	11	0.002	306	315	9	0.024
$cTnI(L160C)_{TAMRA}$	307	312	5	0.039	299	309	10	0.003
$cTnI(S167C)_{TAMRA}$	332	341	9	0.014	324	336	12	0.002
$cTnI(V177C)_{TAMRA}$	293	296	3	0.024	282	273	−9	<0.001
$cTnI(I182C)_{TAMRA}$	320	305	−15	<0.001	305	299	−6	0.034
$cTnI(V189C)_{TAMRA}$	308	300	−8	0.012	298	291	−7	0.025
$cTnI(S200C)_{TAMRA}$	302	285	−17	<0.001	285	277	−8	<0.001
$cTnI(E210C)_{TAMRA}$	315	299	−16	<0.001	297	287	−10	<0.001

[a] ΔFA is Ca^{2+} binding-induced fluorescence anisotropy change in mA.
[b] *p* values obtained from Student's *t* test comparing the anisotropy of the Mg^{2+} state with that of the Ca^{2+} state (with or without S1 present).

cTnC, the fluorescence anisotropy of the IR of cTnI changed insignificantly. This was expected because upon Ca^{2+} binding the IR switches from interacting with the actin filament to interacting with the central helix of cTnC, resulting in little change in its regional structural mobility.

The other two functional regions of cTnI showed fluorescence anisotropies in the absence of Ca^{2+} ranging from 293 to 332 mA. However, the fluorescence anisotropy of the RR (including residues Cys-151, Cys-160, and Cys-167) in the presence of Ca^{2+} significantly increased by 5–11 mA ($p < 0.05$ in all cases), whereas the fluorescence anisotropy of the MD (including residues Cys-182, Cys-189, Cys-200, and Cys-210) significantly decreased by 8–17 mA ($p < 0.001$ for residues Cys-182, Cys-200, and Cys-201; $p < 0.05$ for residue Cys-189). These changes are consistent with the Ca^{2+}-induced changes in structural dynamics expected for these regions. The RR is expected to have a highly flexible structure in the absence of Ca^{2+} due to its relative lack of interaction with other thin filament protein interfaces in that state. Binding of Ca^{2+} to cTnC induces a strong interaction between the N-domain of cTnC and the RR of cTnI, which should significantly dampen its structural dynamics. The MD of cTnI interacts with the actin filament in the absence of Ca^{2+}, resulting in low flexibility for the region. Upon Ca^{2+} binding, the region and particularly its C terminus became highly flexible, suggesting that the MD moved away from the actin filament as expected.

To further test our hypothesis and examine how the structural dynamics of these regions could be affected by strong cross-bridge formation, S1-Mg^{2+}-ADP was introduced to samples as a strong cross-bridge analog. Results in Table 2 show that in the absence of Ca^{2+} strongly bound S1 had an insignificant impact on the anisotropy of the control residue Cys-98 of cTnI but decreased the fluorescence anisotropy of all three C-cTnI functional regions by 6–18 mA ($p < 0.05$), suggesting that strongly bound S1 induced a disengagement of C-cTnI away from actin, leading to more flexibility in the structure of its functional regions. This effect was most pronounced on the IR and the MD, suggesting further that a weakening of the coupling between these regions and actin may be the cause of the apparent disengagement; this is consistent with the ability of strongly bound cross-bridges to activate the thin filament in the absence of calcium. Similarly, comparing the Ca^{2+} state to the Ca^{2+} + S1 state, the anisotropy of all functional regions was decreased due to the presence of S1. This is to be expected as it is known that strongly bound cross-bridges are able to shift tropomyosin on actin from the closed to open positions described by the three-state model of thin filament activation, and this shift would in turn push the binding regions of C-cTnI further away from the actin filament. These results are consistent with previous FRET measurements showing that strongly bound S1 increases distances between C-cTnI and actin (33, 34). Finally, Ca^{2+} binding to cTnC in the presence of strongly bound S1 induced changes in the anisotropies of the labeled regions of C-cTnI that were similar to the case when S1 was absent, implying that even in the presence of strong cross-bridges Ca^{2+} binding is required to fully induce the structural transitions in thin filament regulatory proteins that are associated with activation. At this point, we concluded that, consistent with theory, probe motion reflected the regional conformational dynamics of C-cTnI, validating our hypothesis.

Time-resolved Anisotropy Measurements—The results from steady-state anisotropy measurements thus provided us with a quantitative sense of the total *anisotropy* of each C-cTnI functional region under equilibrium conditions, which depends variously on the global motions of either the thin filament or the core domain of cTn relative to the thin filament; regional, subdomain level flexibility of cTnI; and tumbling of the fluorophore itself. To further assess the contribution of each of these types of motions to the observed total anisotropy and quantitatively isolate the regional component of interest, time-resolved anisotropy measurements were performed. In addition to probing tumbling, the time-resolved fluorescence anisotropies should also reflect 1) the global/domain motion of the protein and 2) the structural flexibility of the region of the protein to which TAMRA is attached as long as the correlation times of these structural motions are close to the time scale of the excited state lifetime of the fluorophore. Because of the large size of the thin filament, the contribution of its global motion to the anisotropy observed during the fluorescence lifetime of the fluorophore should be negligible in time-resolved measurements. Furthermore, although core domain motion could be faster than thin filament motion, core domain motion would still be relatively slow and should affect all regions of C-cTnI equally. Because the correlation times of domain motions may

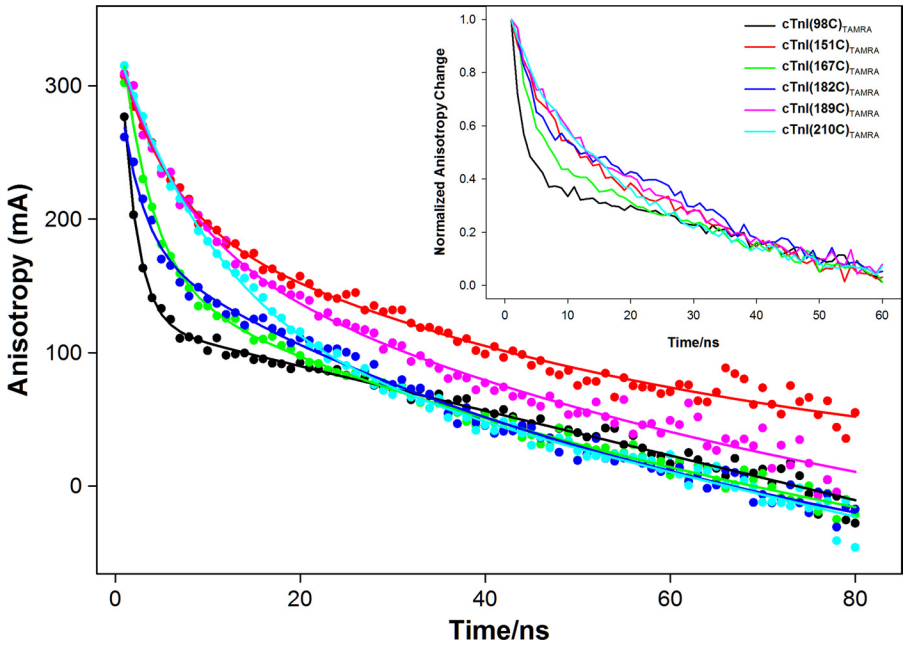

FIGURE 1. **Time-resolved anisotropy decays of selected thin filament samples containing different cTnI single cysteine mutants labeled with TAMRA (see *inset* color legend) in absence of Ca^{2+}.** *Solid circles* are experimental data, and *solid lines* are fitted data. All experimental data were fitted with the two-exponential function given in Equation 4, and recovered anisotropies and correlation times are shown in Table 3. The *inset* graph shows normalized experimental anisotropy decays from which the relative anisotropy correlation time associated with each decay can be readily compared.

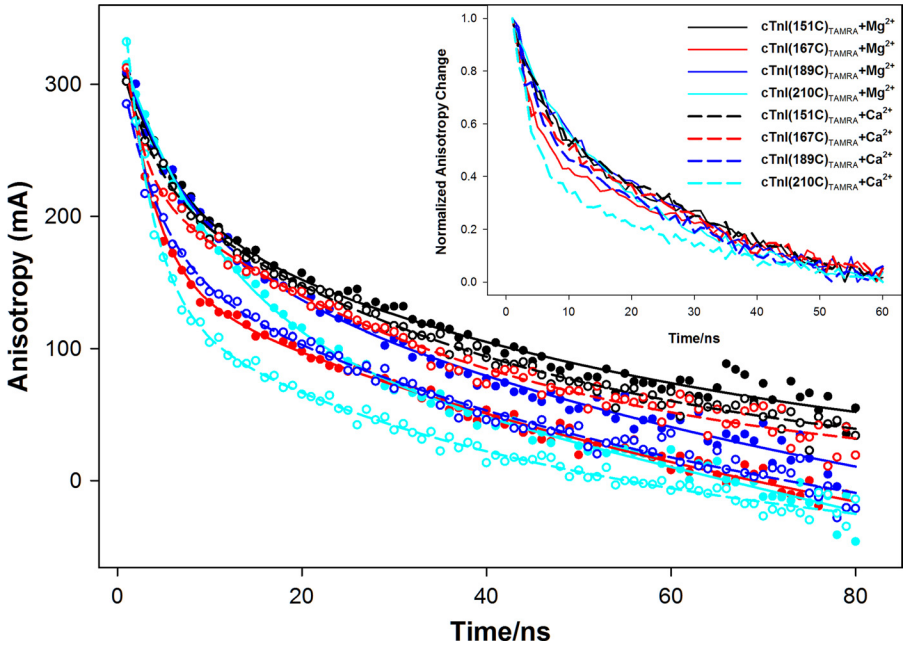

FIGURE 2. **Ca^{2+}-induced changes in time-resolved anisotropy decays of selected thin filament samples containing different cTnI single cysteine mutants labeled with TAMRA (see *inset* color legend) in absence of S1.** *Solid circles* and *hollow circles* are experimental data in the absence of Ca^{2+} and in the presence of Ca^{2+}, respectively. *Solid lines* and *dashed lines* are fitted equations for samples in the absence and presence of Ca^{2+}, respectively. All experimental data were fitted with the two-exponential function given in Equation 4, and recovered anisotropies and correlation times are given in Table 3. The *inset* graph shows normalized experimental anisotropy decays from which the relative anisotropy correlation time associated with each decay can be readily compared.

generally be expected to fall in the range of ns to μs (35), it was expected that the major contributors to time-resolved anisotropy would be regional protein flexibility and fluorophore tumbling.

Fig. 1 shows a typical example of the anisotropy decays of selected thin filament samples containing cTnI (*i.e.* Cys-98) or cysteine-less cTnI mutants S151C, S167C, I182C, V189C, and E210C labeled with TAMRA. Fig. 2 shows Ca^{2+}-induced anisotropy decays of selected thin filament samples containing cysteine-less cTnI mutants S151C, S167C, V189C, and E210C labeled with TAMRA. Fitting the obtained anisotropy decays with Equation 4 gave two correlation times, one in the range of 1.44–5.9 ns and the other in the range of 32.7–65 ns. The specific correlation times and associated amplitudes obtained from

TABLE 3

Fluorescence anisotropy correlation time of TAMRA-labeled cTnI within reconstituted thin filament in presence/absence of strongly bound S1

Samples	Correlation Time(ns)|*Anisotropy(mA)* (thin filament)		Correlation Time(ns)|*Anisotropy(mA)* (thin filament + S1-ADP)	
	Mg^{2+}	Ca^{2+}	Mg^{2+}	Ca^{2+}
$cTnI(98C)_{TAMRA}$	**65.6** | ***33.3*** 1.64 | *309.0*	**64.9** | ***43.3*** 1.86 | *293.2*	**59.9** | ***37.3*** 1.76 | *294.0*	**57.6** | ***33.7*** 1.79 | *299.2*
$cTnI(130C)_{TAMRA}$	**58.1** | ***107.2*** 3.23 | *264.3*	**50.2** | ***117.2*** 2.27 | *275.9*	**49.6** | ***154.5*** 3.03 | *174.1*	**44.8** | ***135.9*** 2.32 | *184.3*
$cTnI(145C)_{TAMRA}$	**60.7** | ***214.4*** 2.69 | *114.7*	**51.6** | ***197.3*** 3.34 | *138.6*	**56.8** | ***172.5*** 2.01 | *101.3* <0.01 | *0.018*	**47.8** | ***183.5*** 2.78 | *105.6*
$cTnI(151C)_{TAMRA}$	**56.9** | ***201.7*** 4.37 | *118.4*	**53.9** | ***231.1*** 3.65 | *98.2*	**45.4** | ***197.3*** 3.01 | *104.3*	**43.1** | ***189.2*** 2.18 | *103.1*
$cTnI(160C)_{TAMRA}$	**35.5** | ***164.4*** 2.94 | *128.6*	**50.4** | ***195.1*** 3.31 | *107.1*	**29.8** | ***166.3*** 2.63 | *104.2*	**44.9** | ***171.8*** 3.38 | *88.3*
$cTnI(167C)_{TAMRA}$	**38.3** | ***175.6*** 2.30 | *159.1*	**59.5** | ***219.9*** 3.71 | *122.6*	**36.5** | ***142.5*** 2.09 | *162.1*	**48.8** | ***187.8*** 2.76 | *108.9*
$cTnI(177C)_{TAMRA}$	**31.6** | ***164.8*** 1.44 | *139.2*	**33.9** | ***173.2*** 1.81 | *123.7*	**28.8** | ***164.4*** 2.01 | *102.6*	**29.9** | ***171.1*** 2.07 | *98.1*
$cTnI(182C)_{TAMRA}$	**57.8** | ***181.3*** 3.45 | *138.1*	**33.8** | ***153.0*** 2.21 | *157.5*	**42.2** | ***165.9*** 3.11 | *135.7*	**26.2** | ***135.1*** 2.08 | *160.4*
$cTnI(189C)_{TAMRA}$	**57.8** | ***196.0*** 5.90 | *103.8*	**37.5** | ***160.6*** 3.05 | *141.7*	**44.3** | ***153.8*** 3.53 | *104.1*	**29.2** | ***136.4*** 2.25 | *107.9*
$cTnI(200C)_{TAMRA}$	**55.3** | ***201.6*** 3.21 | *103.2*	**32.7** | ***154.3*** 2.11 | *135.8*	**42.2** | ***189.2*** 3.31 | *96.8*	**31.5** | ***163.8*** 2.01 | *102.1*
$cTnI(210C)_{TAMRA}$	**59.9** | ***215.5*** 3.22 | *102.4*	**29.2** | ***160.3*** 1.98 | *138.7*	**49.0** | ***197.5*** 3.29 | *93.7*	**27.1** | ***164.3*** 2.01 | *116.7*

these fittings are given in Table 3. The longer, or slow motion, correlation time (Table 3, boldfaced) corresponds to the slower dynamics associated with regional protein structure, whereas the shorter, or fast motion, correlation time corresponds to the rapid tumbling of the fluorophore. It is noted that the observed correlation times (32.7–65 ns) associated with regional protein structural dynamics are significantly longer than the fluorescence lifetime (3–5 ns) of TAMRA. This may limit the accuracy of the longer correlation times because only limited portions of the regional structural dynamics of the protein were sampled during the fluorescence lifetime of the probe. Even with this limitation, our results enable us to acquire quantitative information associated with region structural dynamics of cTnI in the reconstituted samples. As mentioned previously, the endogenous Cys-98 of cTnI labeled with TAMRA was used as an internal reference to distinguish the contribution of fluorophore tumbling to the observed anisotropy. Because Cys-98 is contained in the rigid cTnI-cTnT extended helix of the core domain (17), the anisotropy measured for TAMRA attached to Cys-98 should be primarily caused by fluorophore tumbling. As expected, the anisotropy decay for the reference Cys-98 of cTnI was dominated by the fast motion correlation time and showed no significant change in response to Ca^{2+}. Thus, we attributed the fast motion correlation time to fluorophore tumbling on the surface of the thin filament.

Analysis of the anisotropy decays from probes located within the IR suggested that based on the amplitudes α_i in the absence of Ca^{2+} the relative contribution from the slow motion correlation time to total anisotropy became significantly increased as one proceeds from the N terminus (one-third at Cys-130) to the C terminus (two-thirds at Cys-145 and Cys-151). Ca^{2+} binding to cTnC generally decreased the slow motion correlation times associated with the IR from 56.9–60.7 to 50.2–53.9 ns without significantly changing associated amplitudes. The IR of C-cTnI is thought to have a flexible structure and is known to interact with actin and cTnC in the absence and presence of Ca^{2+}, respectively. Interestingly, the slow motion correlation times recovered from the anisotropy decays suggest that the inherent flexibility of the IR is dampened by these interactions such that the region has a similar low flexibility in both the Ca^{2+} and Mg^{2+} states. Compared with the IR, the slow motion correlation times from probes attached to the RR (Cys-160 and Cys-167) were much faster (35.5–38.3 ns) in the absence of Ca^{2+}, suggesting an increased flexibility in structure. However, in the presence of Ca^{2+}, the slow motion correlation time increased to 50.4–59.5 ns, reflecting decreased flexibility. This was expected because Ca^{2+} binding to cTnC induces a strong interaction between the RR of C-cTnI and the N-domain cTnC, which would tend to reduce the flexibility of the RR. Based on the amplitudes associated with the slow and fast motion correlation times, the anisotropy decays observed for the RR became more dominated by regional dynamics when Ca^{2+} was present.

Binding of Ca^{2+} to the regulatory site of cTnC induced different changes in the correlation times associated with the MD of C-cTnI *versus* the IR and RR. In the absence of Ca^{2+}, the slow motion correlation times of TAMRA attached to residues Cys-182, Cys-189, Cys-200, and Cys-210 were relatively slow at 52.8–59.9 ns but in the presence of Ca^{2+} were accelerated to 33.8–37.5 ns. The amplitudes associated with these slow motion correlation times also changed in response to Ca^{2+} binding such that the anisotropy became less dominated by regional dynamics but not to the extent of that seen in Cys-98. The pattern that fits most with this trend in amplitude changes and the trends observed for the amplitude changes of the IR and RR is that the more a labeled residue participates strongly in a protein-protein interaction, the more regional dynamic motion dominates its anisotropy decay. Overall, the changes in the slow motion correlation times and their amplitudes suggested that the MD generally had slow structural dynamics and strong protein-protein interaction in the absence of Ca^{2+} and fast dynamics and weak protein-protein interaction in the presence of Ca^{2+}. However, TAMRA attached to residue Cys-177 showed fast correlation times in both the presence and absence of Ca^{2+}, consistent with its location in a hinge region (15). Taken together, the observed Ca^{2+}-dependent changes in correlation times agree well with the "drag-and-release" mechanism (11, 36, 37), which predicts that 1) the Mg^{2+} state flexibility of the RR will be significantly reduced by the Ca^{2+}-induced strong interaction between the N-cTnC and the RR of cTnI and 2) this interaction between the RR and N-cTnC will pull the IR and the MD away from their binding sites on the actin surface, leading to more flexibility in the MD (15, 16) but similarly low flexibility in the IR due to its interaction with the central helix of cTnC (38, 39).

We also observed that fast motion correlation times depended on biochemical conditions and where TAMRA was positioned within C-cTnI, which could suggest that the tumbling motion of TAMRA was influenced by its surrounding environment. One can envision that as Ca^{2+} signaling induces changes in the structural dynamics and the surrounding spatial environment of the region to which TAMRA is attached these changes are reflected in the fast motion correlation time. This notion is supported by the fact that changes in the fast motion correlation time were correlated with changes in the slow

motion correlation time, the latter of which represents changes in regional flexibility. However, it is also possible that the motion of the core domain of cTn changed relative to the thin filament, which might be expected to change both the fast motion and slow motion correlation times together. Because changes occurred in opposite directions depending on location (*e.g.* RR *versus* MD), this latter interpretation is less likely. Consequently, these observations are most consistent with the notion that the faster the dynamic motion of a protein subdomain or segment is, the more it provides an environment that allows full probe mobility and hence faster tumbling, whereas slow structural dynamics within a region may tend to hinder probe motion.

In terms of the effects of S1-Mg^{2+}-ADP on anisotropy decay, it tended to speed up both fast and slow motion correlation times. This is in accord with our steady-state anisotropy measurements in which we observed significant decreases in the anisotropy of TAMRAs attached to the cysteine residues along C-cTnI in the presence of strongly bound S1. Furthermore, the weights of the longer correlation times of fluorophores attached to each region of cTnI were decreased when S1-ADP-Mg^{2+} was added to the samples (with the exception of Cys-130; see Table 3). It is believed that these changes are caused by a strong interaction between actin and S1 that promotes the movement of tropomyosin from the closed state to the open state. As a consequence of tropomyosin movement, the majority of C-cTnI is disengaged from actin and becomes more flexible. Interestingly, the N terminus of the IR may behave differently by coming into even closer engagement with the actin filament perhaps through contact with tropomyosin, which may aid in triggering relaxation. Finally, binding of Ca^{2+} to cTnC in the presence of strongly bound S1 caused similar changes in both fast and slow motion correlation times at every region of cTnI as compared with that in the absence of strongly bound S1.

Fluorescence Quenching Measurements—The results of our anisotropy measurements revealed that the functional regions of C-cTnI, when incorporated into the thin filament, each had characteristically different Ca^{2+}-dependent conformational dynamics. It is expected that regions with faster dynamics should be more exposed and accessible to solvent molecules than the regions with less flexibility. Hence, to assess regional solvent accessibility under different conditions and further interrogate our hypothesis, fluorescence quenching experiments were performed using IAANS attached to the single cysteine of each cTnI mutant and acrylamide as a neutrally charged quencher molecule. Fig. 3 shows typical examples of the acrylamide-dependent quenching of regional IAANS fluorescence intensity in reconstituted thin filaments and in the presence/absence of Ca^{2+}. Quenching constants (K_{SV}) determined from fitting are shown in Table 4. In the absence of Ca^{2+} (Fig. 3*A*), the RR exhibited the highest slopes, implying that it was more accessible to solvent than the IR and the MD as expected. In the presence of Ca^{2+}, slopes of probes in the RR decreased, whereas slopes of probes in the MD increased significantly, suggesting 1) the onset of the interaction between the RR and N-cTnC, which dampened its solvent accessibility, and 2) cessation of the interaction between the MD and actin, resulting in increased access of the MD to solvent. Hence, these Ca^{2+}-dependent changes in residue accessibility observed for the RR and MD were consistent with the changes in structural dynamics for these regions that were observed in our anisotropy results (Tables 2 and 3).

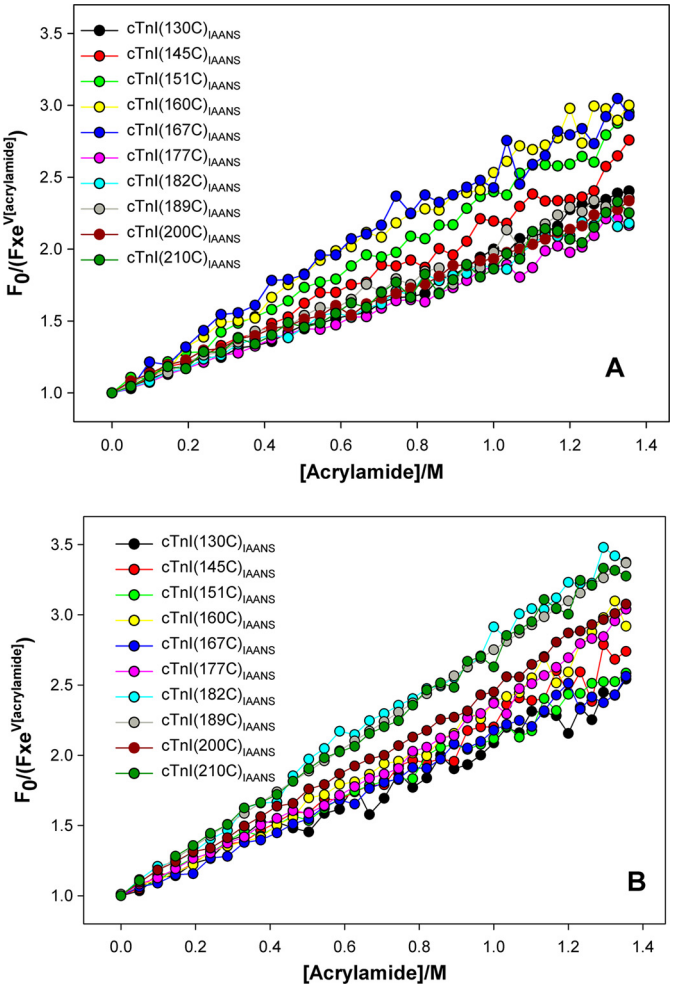

FIGURE 3. **Fluorescence quenching experimental data on reconstituted thin filaments containing different IAANS-labeled single cysteine mutant cTnIs (see *inset* color legend) in absence of Ca^{2+} (*A*) and in presence of Ca^{2+} (*B*).** Each of the quenching curves was fitted to Equation 5 to recover the Stern-Volmer quenching constant (K_{SV}). For the sake of clarity, fitted curves were not plotted in the graphs.

TABLE 4

Results of fluorescence quenching to assess accessibility of each region of C-cTnI within thin filament under different biochemical states

Samples	Fluorescence quenching constant			
	Thin filament		Thin filament + S1-ADP	
	Mg^{2+}	Ca^{2+}	Mg^{2+}	Ca^{2+}
	M^{-1}			
$cTnI(T130C)_{IAANS}$	1.04	1.07	1.17	0.98
$cTnI(L145C)_{IAANS}$	1.20	1.27	1.25	1.18
$cTnI(S151C)_{IAANS}$	1.37	1.14	1.38	1.29
$cTnI(L160C)_{IAANS}$	1.51	1.48	1.47	1.38
$cTnI(S167C)_{IAANS}$	1.43	1.16	1.51	1.32
$cTnI(V177C)_{IAANS}$	0.86	1.15	1.11	1.53
$cTnI(I182C)_{IAANS}$	0.97	1.82	1.23	1.78
$cTnI(V189C)_{IAANS}$	1.00	1.56	1.09	1.67
$cTnI(S200C)_{IAANS}$	0.92	1.51	1.13	1.62
$cTnI(E210C)_{IAANS}$	0.911	1.74	1.16	1.75

When strongly bound S1 was present, fluorescence quenching constants generally increased in the Mg^{2+}-bound state, and this effect was most pronounced for the MD (Table 4). Although this suggests as with our anisotropy results that strongly binding cross-bridges exert a general structural effect on the C-domain of cTnI by shifting C-cTnI away from the actin filament, it further suggests a significantly looser coupling between the MD and actin that may reflect a weakened protein-protein interaction. This same inference could be drawn for the IR but to a lesser extent. However, the effects of Ca^{2+} on the quenching constants seen in the absence of S1 were generally preserved in the presence of S1, suggesting that although strong cross-bridges are able to modulate Ca^{2+}-dependent activation Ca^{2+} is required to fully induce the activation-associated structural transitions in the C-cTnI dynamic state.

Anisotropy Stopped-flow Measurements—Both steady-state and time-resolved anisotropy measurements suggested that when cTnI is incorporated into the thin filament its functional regions in the C-domain each have unique Ca^{2+}-dependent regional structural dynamics that are modulated by S1. Because structure correlates with function, these differences suggest that each functional region may have a unique role in regulating thin filament activation/deactivation. It is therefore desirable to have kinetic information on each of their dynamic state transitions to better understand the specific regulatory role that each region plays. To accomplish this, we used the fluorescence anisotropy stopped-flow technique to examine the kinetics of changes in C-cTnI structural dynamics triggered by Ca^{2+} dissociation. The structural dynamics of the IR were examined by monitoring the fluorescence anisotropy kinetics of TAMRA attached to residue Cys-151; similarly, for the RR, residues Cys-160 and Cys-167 were monitored; and for MD, residues Cys-182, Cys-189, Cys-200, and Cys-210 were examined. These residues were chosen because TAMRA attached to these residues showed relatively large Ca^{2+}-induced changes in steady-state anisotropy (Table 2).

Fig. 4 shows examples of polarized emission and calculated anisotropy kinetic traces of TAMRA attached to residue Cys-151 in response to Ca^{2+} dissociation from cTnC, and Fig. 5 shows results for residue Cys-210. Both anisotropy kinetic traces (Figs. 4*B* and 5*B*) could be described by two phases: a fast phase and a slow phase described by a rate that was approximately an order of magnitude slower than that of the fast phase. The fast phase was interpreted to reflect the kinetics of changes in fluorophore tumbling caused by changes in the local environment, which in turn are associated with C-cTnI structural changes induced by Ca^{2+} dissociation. Accordingly, the slow phase was interpreted to reflect the kinetics of dynamic state transitions involving regional protein structure that occur in response to Ca^{2+} dissociation. These fast and slow transition phases were observed for all seven of the chosen TAMRA-labeled cTnI samples. Rate constants and associated amplitudes recovered from the analysis of all the kinetic traces are summarized in Table 5.

It is expected that the kinetics of changes in fluorophore tumbling should be very fast due to the small size of the fluorophore. For our measurements taken in the absence of strongly bound S1, the observed kinetics of changes in fluorophore tumbling were typically in the range of 346–432 s^{-1}, which accounts for about 29–39% of observed total anisotropy changes. Ca^{2+}-dependent variations in the fluorophore tumbling state that may underlie these changes in anisotropy would be caused by changes in local environments that hinder the free rotation of the probe on the local protein surface to differing degrees. The slower kinetics describing dynamic state transitions that involve the regional structure of C-cTnI accounted for 61–71% of observed total anisotropy changes. These slow kinetic rates varied according to which structural region was being measured. Among the three functional regions, the IR had the slowest transition kinetics induced by Ca^{2+} dissociation (14.1 s^{-1}), whereas the MD had the fastest (77.4–116.8 s^{-1}) with the C terminus exhibiting the fastest transition (116.8 s^{-1}). The rates of dynamic state transitions involving the RR were between that of the IR and MD. Interestingly, the slow rate was 26.8 s^{-1} for TAMRA attached to Cys-160, which is reminiscent of the slower rates of the IR. On the other hand,

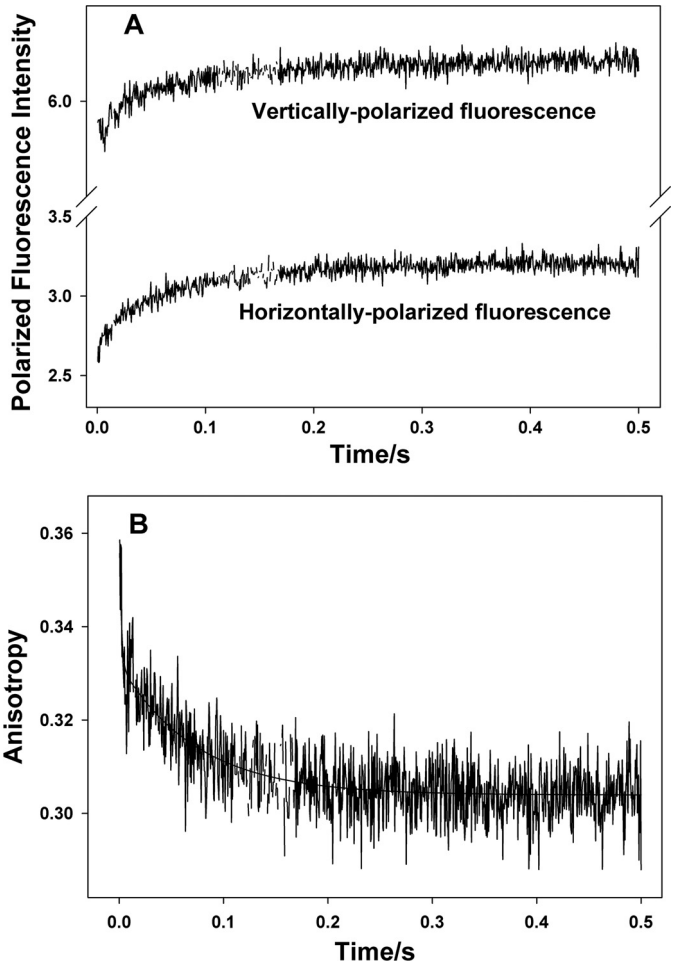

FIGURE 4. **Stopped-flow data on the Ca^{2+} dissociation-induced changes in anisotropy of reconstituted thin filaments containing single cysteine $cTnI(S151C)_{TAMRA}$ in absence of strongly bound S1.** *A*, experimental stopped-flow traces of the polarized fluorescence of TAMRA attached to cTnI(S151C) within the reconstituted thin filament upon Ca^{2+} removal. *B*, the change in anisotropy induced by Ca^{2+} dissociation and calculated from the polarized fluorescence trace shown in *A* using Equation 2. The anisotropy change can be described by a two-exponential function with two kinetic rate constants: one is 346.5 s^{-1} accounting for 31% of the total anisotropy change, and the other is 14.1 s^{-1} accounting for 69% of the total anisotropy change.

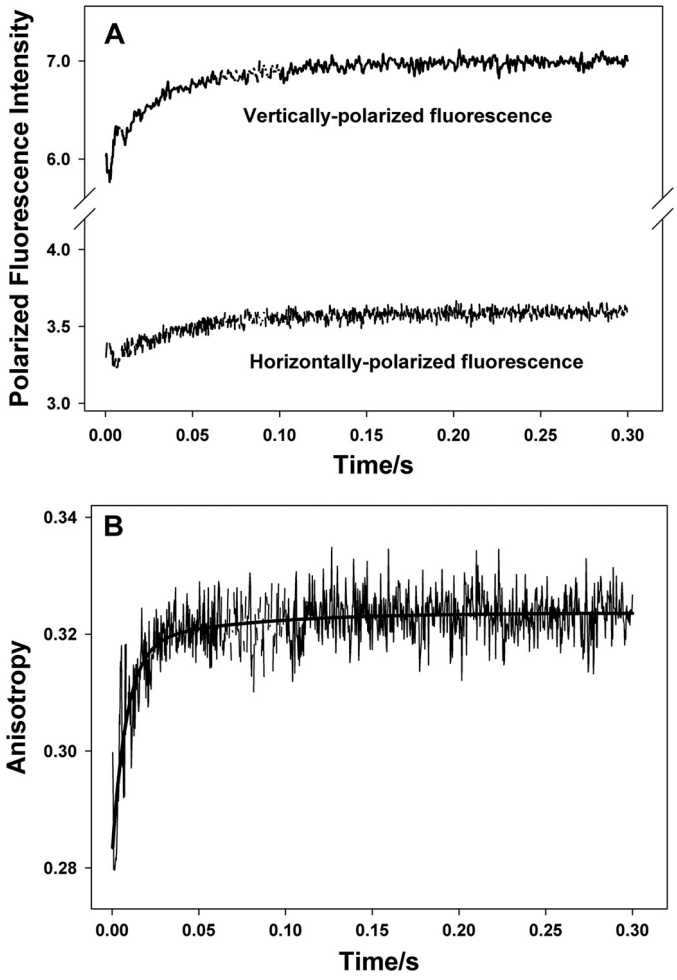

FIGURE 5. **Stopped-flow data on Ca^{2+} dissociation-induced changes in anisotropy of reconstituted thin filaments containing single cysteine cTnI(E210C)$_{TAMRA}$ in absence of strongly bound S1.** *A*, experimental stopped-flow traces of the polarized fluorescence of TAMRA attached to cTnI(E210C) within the reconstituted thin filament upon Ca^{2+} removal. *B*, the change in anisotropy induced by Ca^{2+} dissociation and calculated from the polarized fluorescence trace shown in *A* using Equation 2. The anisotropy change can be described by a two-exponential function with two kinetic rate constants: one is 417.0 s^{-1} accounting for 39% of the total anisotropy change, and the other is 116.8 s^{-1} accounting for 61% of the total anisotropy change.

TABLE 5

Calcium dissociation-induced anisotropy stopped-flow kinetics of TAMRA-labeled cTnI incorporated into reconstituted thin filament with and without S1

	Kinetic rate/amplitude			
	Thin filament		Thin filament + S1-ADP	
Samples	Fast rate	Slow rate	Fast rate	Slow rate
	s^{-1}			
cTnI(S151C)$_{TAMRA}$	346.5/0.31	14.1/0.69	394.3/0.31	10.3/0.69
cTnI(L160C)$_{TAMRA}$	362.0/0.38	26.8/0.62	389.6/0.36	19.8/0.74
cTnI(S167C)$_{TAMRA}$	432.0/0.38	53.2/0.62	393.7/0.38	41.9/0.62
cTnI(V182C)$_{TAMRA}$	376.3/0.29	80.7/0.71	407.2/0.32	61.8/0.68
cTnI(I189C)$_{TAMRA}$	351.9/0.37	77.4/0.63	372.1/0.41	66.3/0.58
cTnI(V200C)$_{TAMRA}$	398.2/0.36	97.3/0.64	412.4/0.38	73.7/0.62
cTnI(E210C)$_{TAMRA}$	417.0/0.39	116.8/0.61	368.2/0.42	89.2/0.58

TAMRA at residue Cys-167, which is next to the fast MD, was described by a faster kinetic rate of 53.2 s^{-1}. This suggests that transitions in the structural dynamics of the RR of cTnI are kinetically influenced by the IR from the N terminus and the MD from the C terminus and may hint at the RR becoming unstructured as it enters the Ca^{2+}-free state. These observed transition kinetics are very close to the kinetics of Ca^{2+} dissociation-induced structural changes of troponin acquired using FRET (40). Altogether, our stopped-flow results support the recently proposed fly casting model (13) and are consistent with the view that Ca^{2+} dissociation induces a structural transition in an unstructured MD that promotes subsequent structural transitions in the RR and IR through "fly casting activity" (41) and that the transition of the RR seems to serve as a kinetic linkage between the transitions of the MD and the IR.

When strongly bound S1 was present during measurements, the transition kinetics of the structural dynamics of the IR slowed significantly from 14.1 to 10.3 s^{-1}. The transition rates of the other two functional regions of C-cTnI were also reduced by 14–26% but without significant changes in amplitudes. These S1-dependent reductions in kinetic rates suggest that the strong cross-bridges formed between S1 and actin may have had a structural impact on the cTnI-binding sites of actin or the movement of tropomyosin, which in turn kinetically affected the dissociation of the RR from N-cTnC and the rebinding of the IR and the MD to actin. The S1-dependent structural impact also affected the kinetics of changes in fluorophore tumbling by 4–14% (Table 5).

DISCUSSION

In the present study, steady-state and time-resolved fluorescence anisotropy, quenching, and anisotropy stopped-flow techniques were used to acquire dynamic and kinetic information associated with the Ca^{2+}- and S1-dependent allosteric changes in C-cTnI when incorporated into the reconstituted thin filament. Our major findings include the following. 1) Each functional region of C-cTnI is not only characterized by unique dynamics but also distinct Ca^{2+}- and S1-dependent transitions in dynamic structural state in a manner consistent with the three-state model of thin filament activation (42) and the drag-and-release (11, 36, 37) and fly casting models (13). 2) Kinetically speaking, the speed of these structural transitions occurs according to the ranking MD > RR > IR where the IR is slow enough to suggest rate competition with cross-bridge cycling. 3) S1 binding is able to modulate the dynamic structural state of C-cTnI independently of Ca^{2+}. 4) Even in the presence of S1, Ca^{2+} is required to fully activate the thin filament by implication from the fact that Ca^{2+} binding in the presence of S1 is required to fully induce structural transitions in C-cTnI associated with activation. 5) Kinetic evidence suggests that the presence of S1 disrupts the interaction between cTnI and actin/tropomyosin. A model summarizing these Ca^{2+}- and S1-dependent changes in the dynamic state of C-cTnI and its dynamic protein-protein interactions within thin filament is presented in Fig. 6. As will be explained further, the combination of points 3, 4, and 5 above also suggests the existence of a fourth state of thin filament activation as recently proposed by Lehrer (22) in which C-cTnI is intimately involved. Thus, this study represents considerable kinetic and dynamics evidence of the central role that C-cTnI plays in thin filament regulation.

The importance of C-cTnI was highlighted recently by the proposal of a fly casting model (13), which posits an important

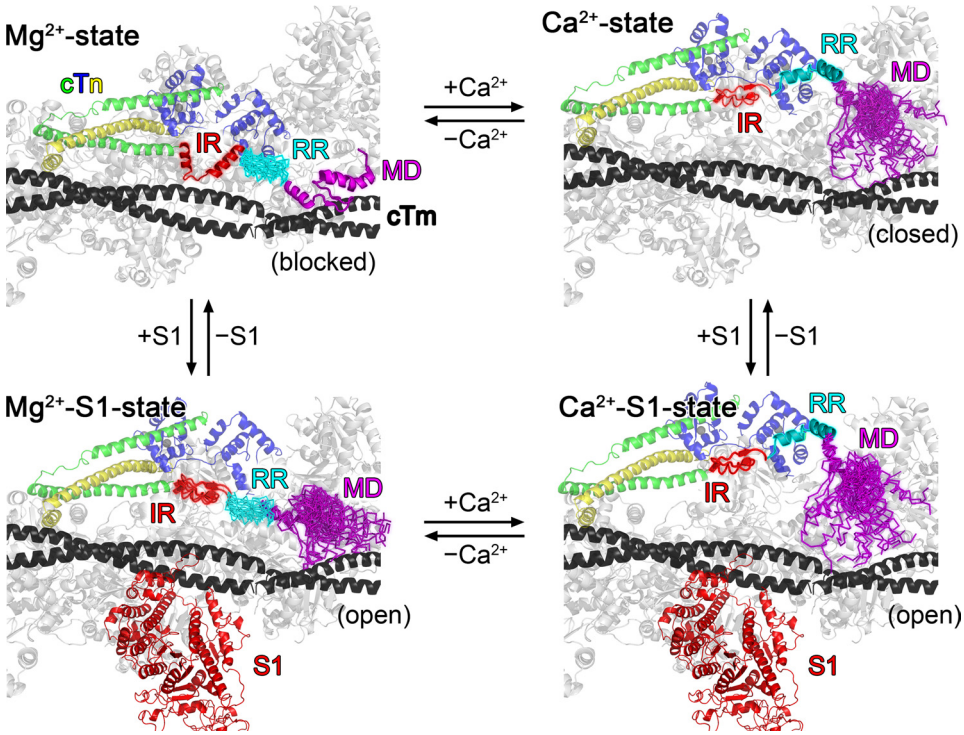

FIGURE 6. **Model for Ca^{2+}- and S1-induced changes in regional structural dynamics in C-domain of cTnI (*green*) and its interactions with other thin filament proteins, including cTnC (*blue*), fragment of cTnT-T2 (*yellow*), actin (*gray*), and tropomyosin (*black*), all of which may be modulated by S1 (*red*).** In the Ca^{2+}-free state with no S1 present, tropomyosin is in the blocked position, and the IR (*glowing red*) and a folded MD (*glowing purple*) of C-cTnI interact with actin, leading to low regional flexibility. In contrast, the RR (*glowing cyan*) maintains no protein interactions and is thus relatively unstructured. Ca^{2+} binding to cTnC in the absence of S1 causes the RR to nucleate into an interaction with cTnC that drags the IR and MD off of actin. Tropomyosin is moved to the closed position, and the MD then becomes unstructured but maintains transient contacts with actin according to the fly casting mechanism, whereas the IR maintains limited flexibility by interacting with the central linker of cTnC. Upon Ca^{2+} dissociation, the MD rapidly nucleates into a binding interaction with actin/tropomyosin that promotes the cessation of the RR-cTnC interaction and the switching of the IR from interacting with cTnC to interacting with actin. Binding of S1 moves tropomyosin to the open position whether in the presence or absence of Ca^{2+}. In the Mg^{2+}-S1 state, C-cTnI interactions with actin/tropomyosin are disrupted, and C-cTnI is biased for interaction with cTnC, thus enhancing the affinity of cTnC for Ca^{2+}, whereas in the Ca^{2+}-S1 state, the RR of cTnI binds to N-cTnC, the IR interacts with the central linker of cTnC, and the MD remains unstructured.

role for the MD of C-cTnI as a rapid initiator of relaxation. This fly casting model was developed based on NMR models derived from studies of free skeletal cTn that showed the MD as intrinsically disordered in solution (16) and therefore able to perform fly casting activity. Our study provides a kinetic picture of the dynamic state structural transitions in C-cTnI induced by Ca^{2+} dissociation that confirms the fly casting model in reconstituted cardiac thin filaments. Similar kinetics were found in a previous study by our laboratory (40) that used FRET to monitor structural transitions involving the IR and RR of C-cTnI and their proximity to cTnC and actin except that here 1) the kinetics presented are generally slower, 2) the MD is characterized in addition to the IR and the RR and is seen to undergo the most rapid structural transitions upon Ca^{2+} dissociation, and 3) the relationship between the structural transitions among C-cTnI functional regions is clearly visualized as in support of the fly casting model, clarifying the two-step structural transition in the thin filament that was seen in our prior FRET study. Furthermore, our anisotropy results presented here support the notion of the MD as unstructured and highly flexible in the Ca^{2+} state even when C-cTnI is incorporated into the thin filament in agreement with a follow-up study from Sykes and co-workers (43) that investigated the structure of a skeletal TnC-TnI chimera using NMR. Thus, our study supports the view of the MD as a rapid initiator of relaxation in the absence of S1; however, the fly casting model did not include any predictions concerning the effect of strong cross-bridges on the proposed mechanism. The fact that the presence of S1 globally slowed C-cTnI structural transitions induced by Ca^{2+} dissociation suggests that Mg^{2+} state interactions between C-cTnI and actin/tropomyosin are disrupted in the presence of S1. Based on our collective results, we propose a revised mechanistic scheme of Ca^{2+}-induced thin filament deactivation as presented in Scheme 2. As in our previously proposed scheme (40), muscle relaxation is suggested to involve a "rapid-then-slow" two-step structural transition of the thin filament at the interface between cTn and actin. The fly casting activity of the MD of C-cTnI is responsible for initiating the rapid first step, and the second slow step involves the "from cTnC/to actin" switching activity of the IR of C-cTnI. However, the presence of S1 disrupts the ability of the MD to nucleate onto actin/tropomyosin, resulting in a greater stabilization of the interaction between the RR of C-cTnI and N-cTnC; thus, the entire two-step process is slowed. Hence, the rapid relaxation role of the MD may be attenuated by strong cross-bridges.

One explanation for the impact of S1 on the kinetics of Ca^{2+} dissociation-induced structural transitions as well as our anisotropy and fluorescence quenching data involving S1 is competition between cross-bridges and C-cTnI for control of the position of tropomyosin on actin. Strong evidence has recently

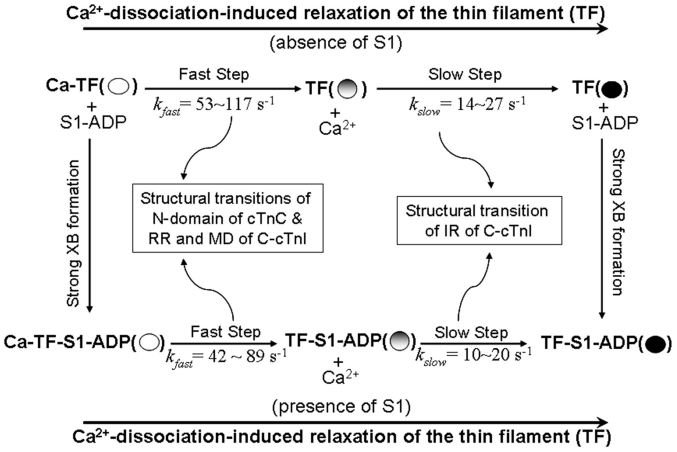

SCHEME 2. **Kinetic model (in support of fly casting mechanism and feedback modulation by S1) of regulatory behavior of thin filament during relaxation.** *TF*, thin filament; *XB*, cross-bridge.

emerged that C-cTnI forms direct contacts with tropomyosin and controls its movement. For example, Lehman and co-workers (44) demonstrated through three-dimensional EM reconstructions that 1) the MD makes direct contact with tropomyosin in the blocked state, 2) upon Ca^{2+} binding, the core domain of Tn directs the movement of tropomyosin into the closed position (45), and 3) transient contacts made by the MD with actin in the Ca^{2+} state help stabilize tropomyosin in the closed position (46). Furthermore, Lehrer and co-workers (47) showed that residue 146 of tropomyosin labeled with 4-maleimidobenzophenone photocross-links with residues 157–163 of C-skeletal TnI in a Ca^{2+}-dependent manner, suggesting that in the blocked state TnI interacts with tropomyosin to lock it on the outer domain of actin. The photocross-linking was inhibited when conducted in the presence of a molar ratio of 1–2:7 S1:actin, demonstrating that S1 is able to disrupt the interaction between TnI and tropomyosin. This is consistent with a prior study by Lehrer and co-workers (48) that showed the same result for the interaction between C-skeletal TnI and actin, suggesting that S1 is able to dissociate C-cTnI from actin and tropomyosin by directly moving tropomyosin to the open state. Thus, the Ca^{2+}-independent and S1-induced movement of tropomyosin to the open state is the most likely explanation for the S1-dependent disruption of Mg^{2+} state interactions between C-cTnI and actin/tropomyosin detected in our anisotropy studies.

This explanation fits well with our data, which suggest unambiguously that the interaction of the MD with actin is disrupted in the Mg^{2+}-S1 state, and shows that the flexibility of the IR is significantly increased. We note two exceptions. 1) The apparent regional flexibility of cTnI is not greatly increased in all cases, perhaps suggesting that the IR switches into a weak interaction with cTnC. 2) Although the correlation times (Table 3) and fluorescence quenching constants (Table 4) for the MD are faster and higher, respectively, in the Mg^{2+}-S1 state than in the Mg^{2+} state, Ca^{2+} is still required even in the presence of S1 to achieve the fastest correlation times and highest fluorescence quenching constants possible for the MD, perhaps suggesting that some form of weaker interaction involving the MD is taking place. We speculate that because the transient contacts of the MD with actin help stabilize tropomyosin in the closed position in the absence of S1 such contacts may continue when S1 holds tropomyosin in the open position. And if transient contacts are maintained between the MD and tropomyosin in the Mg^{2+}-S1 state, then they may be stronger compared with the Ca^{2+} state because the RR remains unbound from N-cTnC. Regardless, it is clear that S1 exerts a Ca^{2+}-independent and disruptive effect on the interaction of C-cTnI with actin/tropomyosin.

If the Mg^{2+} state interaction between C-cTnI and actin/tropomyosin is disrupted, then this begs the question of what then is C-cTnI "doing?" Our kinetics data clearly demonstrate that Ca^{2+} dissociation induces a structural transition in all three functional regions of C-cTnI even in the presence of S1 according to the same ranking in speed as when S1 is absent, although the transitions are significantly and universally slowed. Lehrer (22) recently proposed a fourth state of thin filament activation wherein S1 binds to actin in the absence of Ca^{2+}, shifting tropomyosin to the open position. This dissociates cTnI from actin/tropomyosin and causes cTnI to interact with cTnC to enhance its Ca^{2+} affinity. Our data strongly support the existence of this fourth state. Whether C-cTnI is interacting strongly with cTnC in the Mg^{2+}-S1 state is doubtful because our data suggest that all functional regions of C-cTnI become more flexible in the Mg^{2+}-S1 state relative to the Mg^{2+} state and that Ca^{2+} is still clearly required for the interaction of the RR with N-cTnC even in the presence of S1. We have already speculated that the MD may be maintaining transient contacts with the thin filament in the Mg^{2+}-S1 state (and by implication the Ca^{2+}-S1 state), which would explain why structural transitions in the MD still occur the fastest, compared with the structural transitions of the IR and RR, upon Ca^{2+} dissociation in the presence of S1. Nevertheless, removing the sampling constraints caused by the strong interactions of C-cTnI with actin/tropomyosin may disengage C-cTnI from the thin filament and bias it toward interaction with N-cTnC. Furthermore, when Ca^{2+} dissociation occurs in the presence of S1, the disrupted ability of the MD to nucleate onto the thin filament would result in a greater energetic barrier toward the dissociation of the RR from N-cTnC. Not only would this slow the dissociation of the RR from N-TnC (and the structural transitions of the IR and MD) as seen in our stopped-flow results but it would also enhance the affinity of N-cTnC for Ca^{2+}. For example, the partial truncation of the MD leads to an enhanced Ca^{2+} sensitivity of steady-state isometric tension in rat trabeculae (49, 50). Thus, the role of the MD as a rapid initiator of relaxation may ironically also serve the purpose of indirectly contributing to the modulation of the affinity of cTnC for Ca^{2+} in a manner tuned for regulatory interaction with the cross-bridge cycle.

In conclusion, the results from our study demonstrated the usefulness of anisotropy for monitoring the regional structural dynamics of each of the C-cTnI functional regions. The distinct Ca^{2+}- and S1-dependent structural dynamics and dynamic state transition kinetics obtained for each region were closely correlated to each of their functional roles in regulatory switching in a manner that is consistent with the drag-and-release mechanism, fly casting model, three-state model of thin fila-

ment regulation, and a fourth state of thin filament activation associated with the Mg^{2+}-S1 state. Thus, our results underscore the central role that C-cTnI plays in thin filament regulation. Although it is clear that both Ca^{2+} and S1 binding contribute to the activation state of the thin filament, C-cTnI forms an important and dynamic linkage between Ca^{2+}-dependent regulation and the cross-bridge cycle. Clearly, this linkage must be considered in attempts to understand how mutations in thin filament regulatory proteins may lead to pathology.

REFERENCES

1. Ebashi, S., Endo, M., and Otsuki, I. (1969) Control of muscle contraction. *Q. Rev. Biophys.* **2,** 351–384
2. Farah, C. S., and Reinach, F. C. (1995) The troponin complex and regulation of muscle contraction. *FASEB J.* **9,** 755–767
3. Haselgrove, J. C. (1972) X-ray evidence for a conformational change in the actin-containing filaments of vertebrate striated muscle. *Cold Spring Harbor Symp. Quant. Biol.* **37,** 341–352
4. Huxley, H. E. (1973) Structural changes in the actin- and myosin-containing filaments during contraction. *Cold Spring Harbor Symp. Quant. Biol.* **37,** 361–376
5. Parry, D. A., and Squire, J. M. (1973) Structural role of tropomyosin in muscle regulation: analysis of the x-ray diffraction patterns from relaxed and contracting muscles. *J. Mol. Biol.* **75,** 33–55
6. Dong, W. J., Xing, J., Villain, M., Hellinger, M., Robinson, J. M., Chandra, M., Solaro, R. J., Umeda, P. K., and Cheung, H. C. (1999) Conformation of the regulatory domain of cardiac muscle troponin C in its complex with cardiac troponin I. *J. Biol. Chem.* **274,** 31382–31390
7. Li, M. X., Spyracopoulos, L., and Sykes, B. D. (1999) Binding of cardiac troponin-I147–163 induces a structural opening in human cardiac troponin-C. *Biochemistry* **38,** 8289–8298
8. Dong, W. J., Xing, J., Robinson, J. M., and Cheung, H. C. (2001) Ca^{2+} induces an extended conformation of the inhibitory region of troponin I in cardiac muscle troponin. *J. Mol. Biol.* **314,** 51–61
9. Dong, W. J., Robinson, J. M., Stagg, S., Xing, J., and Cheung, H. C. (2003) Ca^{2+}-induced conformational transition in the inhibitory and regulatory regions of cardiac troponin I. *J. Biol. Chem.* **278,** 8686–8692
10. Kobayashi, T., Kobayashi, M., Gryczynski, Z., Lakowicz, J. R., and Collins, J. H. (2000) Inhibitory region of troponin I: Ca^{2+}-dependent structural and environmental changes in the troponin-tropomyosin complex and in reconstituted thin filaments. *Biochemistry* **39,** 86–91
11. Robinson, J. M., Dong, W. J., Xing, J., and Cheung, H. C. (2004) Switching of troponin I: Ca^{2+} and myosin-induced activation of heart muscle. *J. Mol. Biol.* **340,** 295–305
12. Lehman, W., Craig, R., and Vibert, P. (1994) Ca^{2+}-induced tropomyosin movement in *Limulus* thin filaments revealed by three-dimensional reconstruction. *Nature* **368,** 65–67
13. Hoffman, R. M., Blumenschein, T. M., and Sykes, B. D. (2006) An interplay between protein disorder and structure confers the Ca^{2+} regulation of striated muscle. *J. Mol. Biol.* **361,** 625–633
14. Gordon, A. M., Homsher, E., and Regnier, M. (2000) Regulation of contraction in striated muscle. *Physiol. Rev.* **80,** 853–924
15. Murakami, K., Yumoto, F., Ohki, S. Y., Yasunaga, T., Tanokura, M., and Wakabayashi, T. (2005) Structural basis for Ca^{2+}-regulated muscle relaxation at interaction sites of troponin with actin and tropomyosin. *J. Mol. Biol.* **352,** 178–201
16. Blumenschein, T. M., Stone, D. B., Fletterick, R. J., Mendelson, R. A., and Sykes, B. D. (2006) Dynamics of the C-terminal region of TnI in the troponin complex in solution. *Biophys. J.* **90,** 2436–2444
17. Takeda, S., Yamashita, A., Maeda, K., and Maéda, Y. (2003) Structure of the core domain of human cardiac troponin in the Ca^{2+}-saturated form. *Nature* **424,** 35–41
18. Tripet, B., Van Eyk, J. E., and Hodges, R. S. (1997) Mapping of a second actin-tropomyosin and a second troponin C binding site within the C terminus of troponin I, and their importance in the Ca^{2+}-dependent regulation of muscle contraction. *J. Mol. Biol.* **271,** 728–750
19. Lakowicz, J. R. (1999) *Principles of Fluorescence Spectroscopy*, 2 Ed., p. 285, Kluwer Academic Publishers, New York
20. Brown, M. P., and Royer, C. (1997) Fluorescence spectroscopy as a tool to investigate protein interactions. *Curr. Opin. Biotechnol.* **8,** 45–49
21. Serdyuk, I. N., Zaccai, N. R., and Zaccai, J. (2007) *Methods in Molecular Biophysics: Structure, Dynamics, and Function*, p. 14, Cambridge University Press, Cambridge, UK
22. Lehrer, S. S. (2011) The 3-state model of muscle regulation revisited: is a fourth state involved? *J. Muscle Res. Cell Motil.* **32,** 203–208
23. Dong, W. J., Chandra, M., Xing, J., Solaro, R. J., and Cheung, H. C. (1997) Conformation of the N-terminal segment of a monocysteine mutant of troponin I from cardiac muscle. *Biochemistry* **36,** 6745–6753
24. Smillie, L. B. (1982) Preparation and identification of α- and β-tropomyosins. *Methods Enzymol.* **85,** 234–241
25. Pardee, J. D., and Spudich, J. A. (1982) Purification of muscle actin. *Methods Enzymol.* **85,** 164–181
26. Xing, J., and Cheung, H. C. (1994) Vanadate-induced changes in myosin subfragment-1 from cardiac muscle. *Arch. Biochem. Biophys.* **313,** 229–234
27. Dong, W. J., Jayasundar, J. J., An, J., Xing, J., and Cheung, H. C. (2007) Effects of PKA phosphorylation of cardiac troponin I and strong cross-bridge on conformational transitions of the N-domain of cardiac troponin C in regulated thin filaments. *Biochemistry* **46,** 9752–9761
28. Chandra, M., Kim, J. J., and Solaro, R. J. (1999) An improved method for exchanging troponin subunits in detergent skinned rat cardiac fiber bundles. *Biochem. Biophys. Res. Commun.* **263,** 219–223
29. Liao, R., Wang, C. K., and Cheung, H. C. (1992) Time-resolved tryptophan emission study of cardiac troponin I. *Biophys. J.* **63,** 986–995
30. Dong, W. J., Xing, J., Ouyang, Y., An, J., and Cheung, H. C. (2008) Structural kinetics of cardiac troponin C mutants linked to familial hypertrophic and dilated cardiomyopathy in troponin complexes. *J. Biol. Chem.* **283,** 3424–3432
31. Gómez-Hens, A., and Aguilar-Caballos, M. P. (2003) Stopped-flow fluorescence polarization immunoassay. *Comb. Chem. High Throughput Screen.* **6,** 177–182
32. Dong, W. J., Robinson, J. M., Xing, J., and Cheung, H. C. (2003) Kinetics of conformational transitions in cardiac troponin induced by Ca^{2+} dissociation determined by Förster resonance energy transfer. *J. Biol. Chem.* **278,** 42394–42402
33. Shitaka, Y., Kimura, C., Iio, T., and Miki, M. (2004) Kinetics of the structural transition of muscle thin filaments observed by fluorescence resonance energy transfer. *Biochemistry* **43,** 10739–10747
34. Xing, J., Chinnaraj, M., Zhang, Z., Cheung, H. C., and Dong, W. J. (2008) Structural studies of interactions between cardiac troponin I and actin in regulated thin filament using Förster resonance energy transfer. *Biochemistry* **47,** 13383–13393
35. Goodey, N. M., and Benkovic, S. J. (2008) Allosteric regulation and catalysis emerge via a common route. *Nat. Chem. Biol.* **4,** 474–482
36. Kobayashi, T., and Solaro, R. J. (2005) Calcium, thin filaments, and the integrative biology of cardiac contractility. *Annu. Rev. Physiol.* **67,** 39–67
37. Li, M. X., Wang, X., and Sykes, B. D. (2004) Structural based insights into the role of troponin in cardiac muscle pathophysiology. *J. Muscle Res. Cell Motil.* **25,** 559–579
38. Sykes, B. D. (2003) Pulling the calcium trigger. *Nat. Struct. Biol.* **10,** 588–589
39. Cachia, P. J., Sykes, B. D., and Hodges, R. S. (1983) Calcium-dependent inhibitory region of troponin: a proton nuclear magnetic resonance study on the interaction between troponin C and the synthetic peptide *N*α-acetyl[FPhe106]TnI-(104–115) amide. *Biochemistry* **22,** 4145–4152
40. Xing, J., Jayasundar, J. J., Ouyang, Y., and Dong, W. J. (2009) Förster resonance energy transfer structural kinetic studies of cardiac thin filament deactivation. *J. Biol. Chem.* **284,** 16432–16441
41. Shoemaker, B. A., Portman, J. J., and Wolynes, P. G. (2000) Speeding molecular recognition by using the folding funnel: the fly-casting mechanism. *Proc. Natl. Acad. Sci. U.S.A.* **97,** 8868–8873
42. Maytum, R., Lehrer, S. S., and Geeves, M. A. (1999) Cooperativity and switching within the three-state model of muscle regulation. *Biochemistry* **38,** 1102–1110

43. Julien, O., Mercier, P., Allen, C. N., Fisette, O., Ramos, C. H., Lagüe, P., Blumenschein, T. M., and Sykes, B. D. (2011) Is there nascent structure in the intrinsically disordered region of troponin I? *Proteins* **79,** 1240–1250
44. Galiñska-Rakoczy, A., Engel, P., Xu, C., Jung, H., Craig, R., Tobacman, L. S., and Lehman, W. (2008) Structural basis for the regulation of muscle contraction by troponin and tropomyosin. *J. Mol. Biol.* **379,** 929–935
45. Lehman, W., Galiñska-Rakoczy, A., Hatch, V., Tobacman, L. S., and Craig, R. (2009) Structural basis for the activation of muscle contraction by troponin and tropomyosin. *J. Mol. Biol.* **388,** 673–681
46. Galiñska, A., Hatch, V., Craig, R., Murphy, A. M., Van Eyk, J. E., Wang, C. L., Lehman, W., and Foster, D. B. (2010) The C terminus of cardiac troponin I stabilizes the Ca^{2+}-activated state of tropomyosin on actin filaments. *Circ. Res.* **106,** 705–711
47. Mudalige, W. A., Tao, T. C., and Lehrer, S. S. (2009) Ca^{2+}-dependent photocrosslinking of tropomyosin residue 146 to residues 157–163 in the C-terminal domain of troponin I in reconstituted skeletal muscle thin filaments. *J. Mol. Biol.* **389,** 575–583
48. Zhou, X., Morris, E. P., and Lehrer, S. S. (2000) Binding of troponin I and the troponin I-troponin C complex to actin-tropomyosin. Dissociation by myosin subfragment 1. *Biochemistry* **39,** 1128–1132
49. Narolska, N. A., Piroddi, N., Belus, A., Boontje, N. M., Scellini, B., Deppermann, S., Zaremba, R., Musters, R. J., dos Remedios, C., Jaquet, K., Foster, D. B., Murphy, A. M., van Eyk, J. E., Tesi, C., Poggesi, C., van der Velden, J., and Stienen, G. J. (2006) Impaired diastolic function after exchange of endogenous troponin I with C-terminal truncated troponin I in human cardiac muscle. *Circ. Res.* **99,** 1012–1020
50. Tachampa, K., Kobayashi, T., Wang, H., Martin, A. F., Biesiadecki, B. J., Solaro, R. J., and de Tombe, P. P. (2008) Increased cross-bridge cycling kinetics after exchange of C-terminal truncated troponin I in skinned rat cardiac muscle. *J. Biol. Chem.* **283,** 15114–15121